ADVANCED HEALTHCARE MATERIALS
www.advhealthmat.de

Nanogenerator for Biomedical Applications

*Hongqing Feng, Chaochao Zhao, Puchuan Tan, Ruping Liu, Xin Chen, and Zhou Li**

In the past 10 years, the development of nanogenerators (NG) has enabled different systems to operate without external power supply. NG have the ability to harvest the mechanical energies in different forms. Human body motions and activities can also serve as the energy source to drive NG and enable self-powered healthcare system. In this review, a summary of several major actual applications of NG in the biomedical fields is made including the circulatory system, the neural system, cell modulation, microbe disinfection, and biodegradable electronics. Nevertheless, there are still many challenges for NG to be actually adopted in clinical applications, including the miniaturization, duration, encapsulation, and output performance. It is also very important to further combine the NG development more precisely with the medical principles. In future, NG can serve as highly promising complementary or even alternative power suppliers to traditional batteries for the healthcare electronics.

1. Introduction

Self-powered system is a system that can work and function without an external power supply. In the past 10 years, there has been tremendous progress in the development of nanogenerators (NG) for self-powered systems. Many types of NG have been fabricated successfully, converting various mechanical energy into electricity.[1–4]

In consideration that more and more implantable or wearable healthcare electronics have been applied in human bodies, the development of NG-based self-powered medical devices is an attractive approach. However, to actually apply NG in human or animal bodies, many considerations need to be taken into account. The applications of the NG in vivo and in vitro are distinct. First, it is important to make sure of the biocompatibility and nontoxicity of the NG materials and the corresponding circuit.[5] Second, the structure of the NG needs to be carefully designed to fit for the narrow and irregular space inside the body.[6] Third, the sensitivity and efficiency of the NG need to be very high, because the in vivo movements are usually very gentle at a small amplitude.

In this review, we first give a brief description of the NG technologies. Then, we summarize the detailed specific results of several major actual applications of NG in the biomedical fields (**Figure 1**). NG can serve as highly promising, complementary, or even alternative power suppliers to traditional batteries for the implantable or wearable biomedical devices.

2. Working Mechanism of NG

There are two types of NG according to their respective electricity generation principles, the piezoelectric nanogenerator (PENG) and the triboelectric nanogenerator (TENG). The origin of NG was discovered to base on Maxwell's displacement current theory.[7]

2.1. PENG

The PENG is composed of materials with piezoelectric effect, flexible substrates, and connecting electrodes.[8–10] Piezoelectric effect is a phenomenon that produces internal electric potential, which is induced by the generation of electric dipole moments under an action of stress. Taking the wurtzite-structured ZnO crystal as an example, the tetrahedrally coordinated Zn^{2+} and O^{2-} are arranged layer by layer along the *c*-axis (**Figure 2**A). The charge centers of the anions and cations coincide with each other without stress action. When an external force is applied on one vertex of the tetrahedron, electric dipole is formed due to the dislocation of negative and positive charge centers (Figure 2B). Moreover, a constructive add-on to the dipole moments created by all units in the crystal creates a piezoelectric field, which results in a potential difference along the strained direction of the crystal.[11,12] This is the piezoelectric potential (piezopotential) (Figure 2C). Once the crystal is connected to an external load, the electrons in the circuit are driven to flow to partially screen the piezoelectric potential. Therefore, a current pulse flowing through the external circuit is continuously produced when the piezoelectric potential is altered periodically by applying a dynamic external force.[13] This is the general mechanism of PENG (Figure 2D). The selection of various biocompatible piezoelectric materials, and design and capsulation of devices are main factors according to biomedical applications.

Dr. H. Feng, C. Zhao, P. Tan, Prof. Z. Li
Beijing Institute of Nanoenergy and Nanosystems
Chinese Academy of Sciences
Beijing 100083, P. R. China
E-mail: zli@binn.cas.cn
Dr. H. Feng, C. Zhao, P. Tan, Prof. Z. Li
School of Nanoscience and Technology
University of Chinese Academy of Sciences
Beijing 100049, P. R. China
Dr. R. Liu, X. Chen
Beijing Institute of Graphic Communication
Beijing 102600, P. R. China
The ORCID identification number(s) for the author(s) of this article can be found under https://doi.org/10.1002/adhm.201701298.

DOI: 10.1002/adhm.201701298

Figure 1. Several major applications of NG in the biomedical fields.

Dr. Hongqing Feng received her Bachelor's Degree and Doctor's Degree in Peking University, Beijing, China. She is currently working as the Assistant Professor at Beijing Institute of Nanoenergy and Nanosystems, Chinese Academy of Science. Her research interest includes antibacterial technologies and implantable nanogenerators.

Chaochao Zhao received his Bachelor's Degree and Master's Degree in Hebei University of Science and Technology, China. He is currently pursuing the Ph.D. degree at Beijing Institute of Nanoenergy and Nanosystems, Chinese Academy of Sciences. His research work is focusing on the application of nanogenerator on drug delivery and self-powered biomedical systems.

Prof. Zhou Li received his Ph.D. from Peking University in Department of Biomedical Engineering in 2010, and Bachelor's Degree from Wuhan University in 2004. He joined School of Biological Science and Medical Engineering of Beihang University in 2010 as an Associate Professor. Currently, he is a Professor in Beijing Institute of Nanoenergy and Nanosystems, Chinese Academy of Sciences. His research interests include nanogenerators, in vivo energy harvesters, self-powered medical devices, and biosensors.

2.2. TENG

The fundamental working principle of TENG is based on the coupling of contact electrification and electrostatic induction. It is generally accepted that when dissimilar materials contact with each other, chemical bonds will be formed between the interfaces of these materials, and then charges, which can be electrons, ions, or molecules, will be transferred from one material to another due to their different ability of capturing electrons. These contact-induced triboelectric charges can generate a potential drop when the two surfaces are separated by a mechanical force, which can drive electrons to flow between the two electrodes built on the top and bottom surfaces of the two materials. In this way, the mechanic energy that provides contact and separates variation is converted into electricity.[14] On the basis of this principle, four kinds of TENGs with different modes have been established.

2.2.1. Vertical Contact–Separation Mode

The vertical contact–separation mode is the first invented operation mode for TENG as shown in **Figure 3**A. Two films with different dielectric properties are stacked face to face, and metallic electrode materials are deposited on the outer surfaces of the friction layers. The physical contact creates opposite charges between the surfaces of these two dielectric films because of different electron affinity (at least one is dielectrics). Subsequently, upon releasing the external force, two friction films are separated by a small gap in the vertical direction, which generates an electric potential drop across the previous contacted surfaces to drive the free electrons to flow through the external connected circuit. Once the gap becomes closed, the electric potential created by triboelectric effect disappears and the electrons flow backward.[15] This mode has high instantaneous power density, simple structure design, and convenience of packaging, which provide several unique advantages for implantable and wearable devices.

2.2.2. Lateral Sliding Mode

As shown in Figure 3B, lateral sliding mode has the same structure as the vertical contact–separation mode. When the

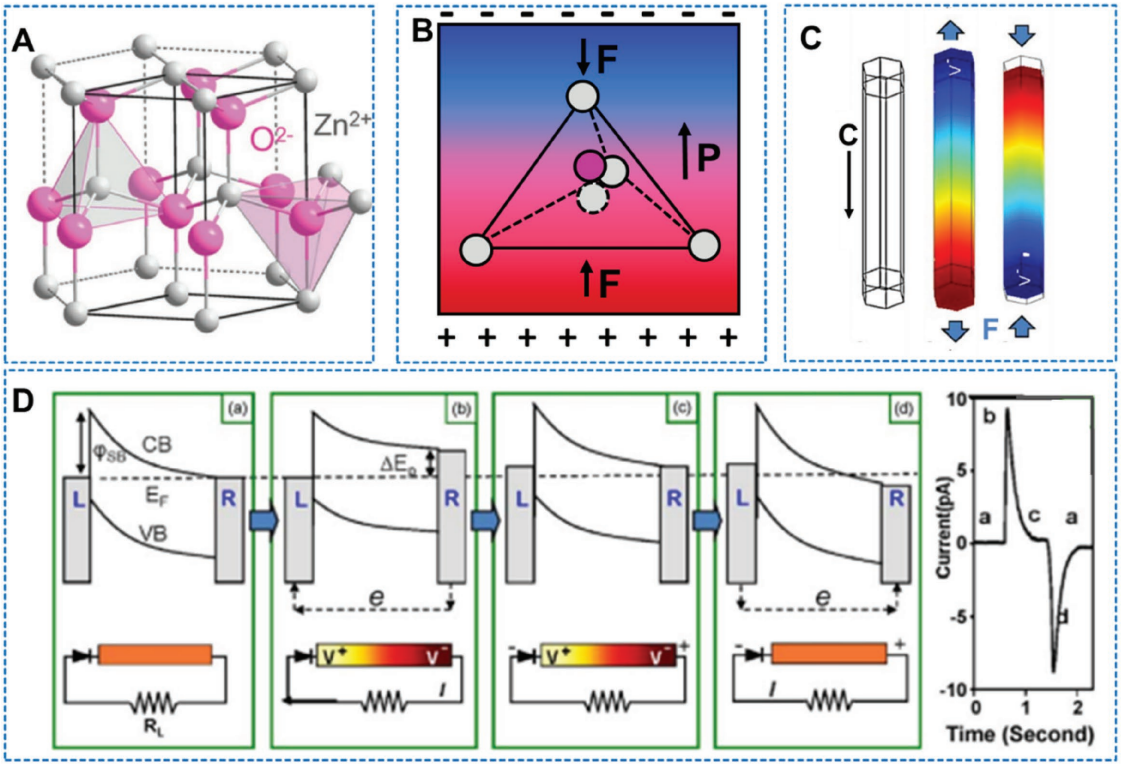

Figure 2. Mechanism of PENG. A) Atomic model of the wurtzite-structured ZnO. B) Piezopotential of a stretched ZnO nanowire. C) Numerical calculation of the piezoelectric potential distribution in a ZnO nanowire under axial strain. Reproduced with permission.[11] Copyright 2017, Elsevier. D) Current generation mechanism explained with energy band diagram of the cyclically stretched nanowire. Reproduced with permission.[11] Copyright 2017, Elsevier.

surfaces of two materials with different triboelectric polarities contact with each other, opposite charges are generated due to the triboelectrification effect. When separation takes place in the sliding direction, triboelectric charges are not completely compensated at the dislocated areas, resulting in the generation of electric charges on the surface. With periodical sliding back and forth, the TENG will drive electrons to flow alternatively across the top and bottom electrodes in order to screen the electric drop induced by the triboelectric charges. Compared with the vertical contact–separation

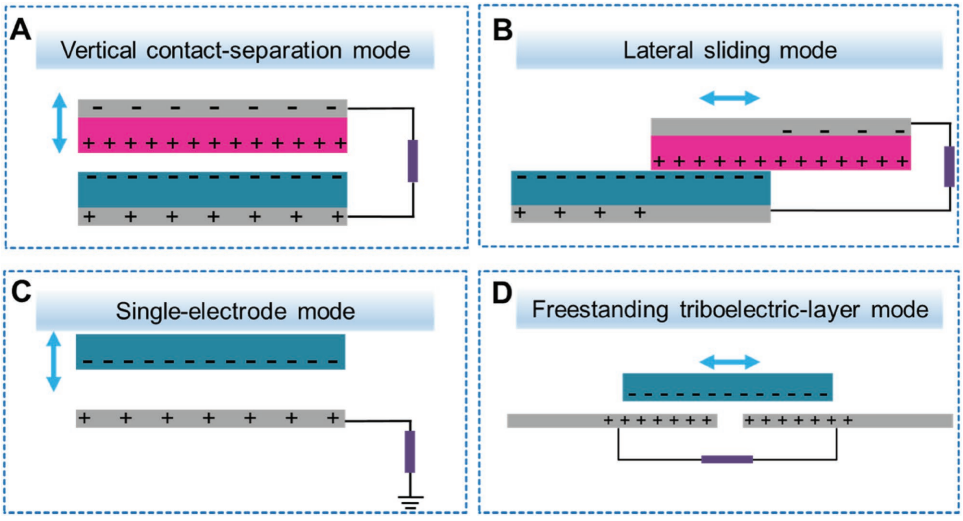

Figure 3. The four fundamental working modes of TENGs. A) The vertical contact–separation mode. B) The lateral sliding mode. C) The single-electrode mode. D) The freestanding triboelectric-layer mode.

mode, this sliding charge separation–contact mode offers more efficient charge transfer. Moreover, various rotation modes such as planar,[15] disk,[16] and cylindrical[17] have been developed, which are widely used in motion sensors and velocity sensors.

2.2.3. Single-Electrode Mode

These two above-mentioned modes generally contain two electrodes interconnected by an external load, which limits their versatility and applicability of energy harvesting from a frequent moving object. On the contrary, single-electrode mode is invented to work independently and can be moved freely. This mode is composed of a moving object and an electrode layer connected to the ground. When the top object approaches to and/or departs from the bottom electrode, it would change the local electrical field distribution, leading to electron flow between the ground and the bottom electrode to match the potential change (Figure 3C). Both vertical contact-mode and lateral sliding-mode, and even the hybridization of these two modes have been applied.[18,19]

2.2.4. Freestanding Triboelectric-Layer Mode

The freestanding triboelectric-layer mode is consisted of two symmetric electrodes underneath a dielectric layer, and the size of the electrodes is of the same order as that of the moving object (Figure 3D). Besides, there is a small gap between the object and the electrodes. Provided the object is precharged by a triboelectric process, with the object is approaching to and/or departing from the electrodes, an asymmetric charge distribution via induction in the media is generated, which causes the electrons to flow from one electrode to another in order to screen the unbalanced potential distribution. The back and forth movement of the electrons between the paired electrodes produces an alternating current output. In this working mode, no direct physical contact between the two triboelectric layers can be realized, which can prolong the lifetime of TENG and is more advantaged for self-powered vibration sensor.[20,21]

In the past 10 years, the design of piezoelectric NG has evolved from the ZnO nanowires (NWs),[22–25] nanocomposite such as $ZnSnO_3$ or $BaTiO_3$,[26–28] to thin films such as polyvinylidene fluoride (PVDF), poly(vinylidenefluoride-*co*-trifluoroethylene), $Pb(Zr_xTi_{(1-x)})O_3$ (PZT), $(1-x)Pb(Mg_{1/3}Nb_{2/3})O_3$–$xPbTiO_3$ (PMN–PT), or lead-free $NaKNbO_3$.[29–33] These development has paved the way for higher output, better conformal property, as well as enhanced miniaturization and safety for PENG, suggesting a tremendous potential to be applied to various medical devices in vivo directly. Besides, based on the conjunction of triboelectrification and electrostatic induction between two different materials, TENG has also shown many advantages, such as high voltage output, lightweight, low cost, and easy fabrication. Fundamentally, any two materials with different electron affinity can be used for preparing TENG. From this perspective, tremendous progress has been made on the output performance, flexibility, biocompatibility, sensitivity, and cost of the device for TENG.[34–37] Most recently, green and recycle TENG or integrated hybrid TENG, capable of harvesting both mechanical and thermal energy, has also been developed.[38,39] Together with the PENG, TENG has become a rising star and provides new options for self-powered biomedical systems.

3. NG Application in the Circulatory System

The circulatory system is also known as the cardiovascular system or the vascular system. Human cardiovascular system is composed of the heart, blood vessels, and blood. The heart pumps oxygenated blood to the body and deoxygenated blood to the lungs. There are four chambers in a heart: left atrium, left ventricle, right atrium, and right ventricle. The right atrium is the upper chamber of the right side of the heart. The deoxygenated blood is returned to the right atrium, passed into the right ventricle, and pumped through the pulmonary artery to the lungs for re-oxygenation and removal of carbon dioxide. Then the newly oxygenated blood is pumped into the left atrium from the lungs, passed into the strong left ventricle, and pumped through the aorta to the different organs of the body. The endless and rhythmical pumping of the four chambers and the artery enable the systemic and pulmonary circulation, and are crucial for one to maintain his life. The cardiovascular system can serve as both the power source and modulation targets of the NG. Therefore, the cardiac system has been the most extensively studied system with regard to NG application up to now. These results demonstrate feasible approaches to scavenge the biomechanical energy, such as heart beating, muscle stretching, or aorta contracting to provide energy for implantable or wearable medical devices.

3.1. Pacemakers

Artificial cardiac pacemakers, which use electrical impulses to stimulate the heart muscles and regulate heartbeat, have made crucial contributions to the patients with sick sinus syndrome or heart block. With the help of pacemakers, abnormal heart rate, which may result in syncope, angina, dizziness, and even heart failure, can become well controlled clinically.[40] However, due to the limitation of the battery lifespan, surgery is needed every 7–10 years to replace the artificial pacemaker implanted beneath chest skin.[41] This brings in much inconvenience, including surgery risk, long healing process, and potential infection. Self-powered energy supply can be an attractive approach to address this challenge, because it can avoid the necessity of replacement surgery and prolong the sustainability of implantable biomedical devices.

Both PENG and TENG have been developed to convert the mechanical energy of heart beat to the electricity supply for pacemakers. Generally, both of them have their specific advantages and drawbacks. Piezoelectric NG are more robust and endurable to long-term repeat of bending and releasing, but the outputs are relatively low. Triboelectric NG can produce higher output, but they need to be encapsulated to protect them from water or liquid leaked into the triboelectric layers, which in turn

hampers the flexibility and the output of the NG. The details are discussed in the following sections.

Li et al. in 2010 demonstrated the first in vivo application of a single-wire generator (SWG) for harvesting biomechanical energy inside a live animal (**Figure 4**A).[42] The piezoelectric ZnO NW had a diameter of 100–800 nm and a length of 100–500 mm. The two ends of the NW were tightly fixed to the surface of a flexible polyimide substrate with silver paste and connected to two lead wires, making Schottky contact at one end and Ohmic contact at the other. The entire device was

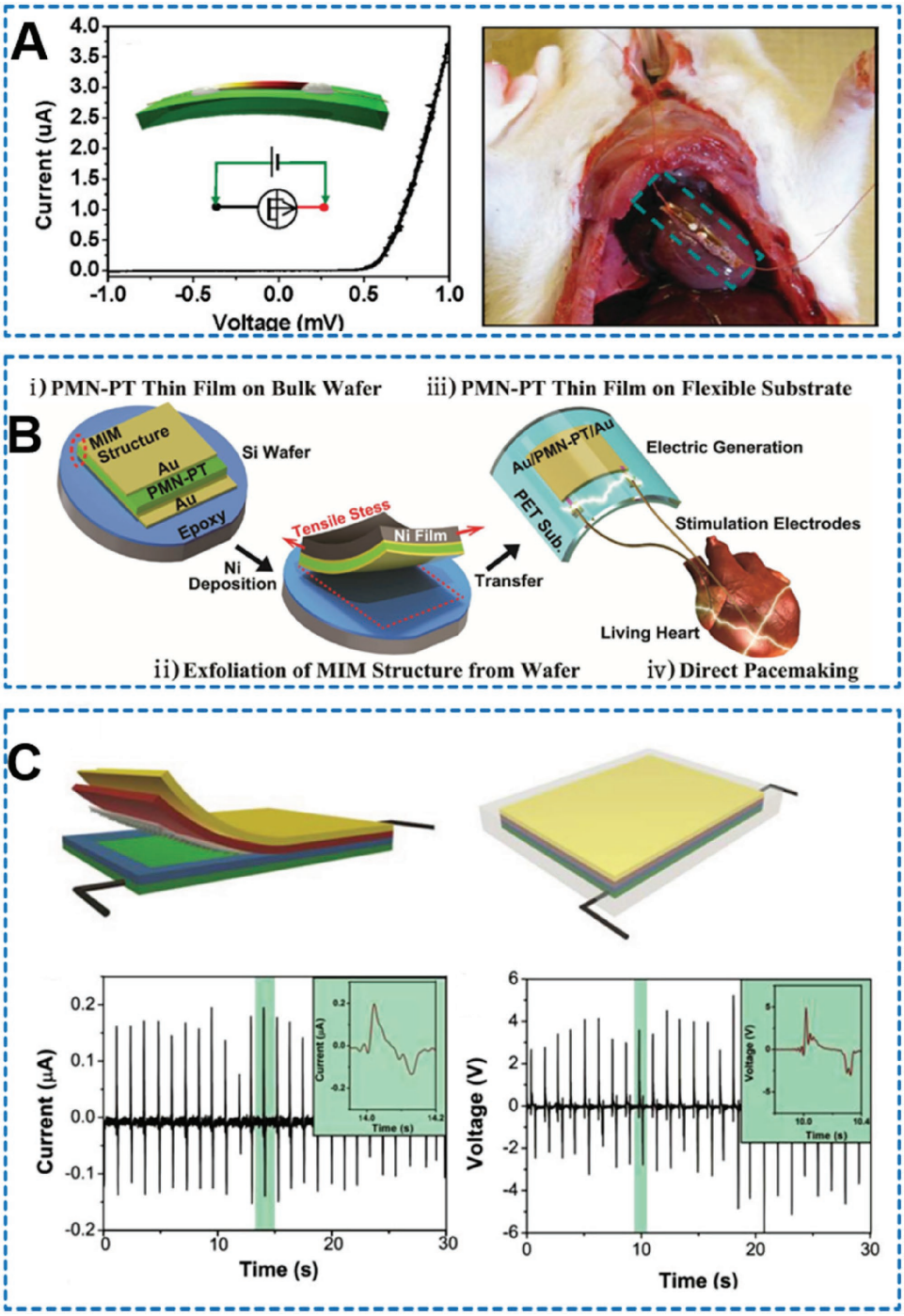

Figure 4. The development of in vivo muscle-driven NG to be the energy supplier for pacemakers. A) The single ZnO nanowire PENG generated a V_{OC} of about 3 mV and an I_{SC} of about 30 pA after implantation. Reproduced with permission.[42] Copyright 2017, John Wiley & Sons. B) The PMN–PT based PENG could generate a maximum output of 8.2 V and 145 μA. Reproduced with permission.[43] Copyright 2017, John Wiley & Sons. C) The first TENG applied in vivo, which generated an output of about 3.73 V and 0.14 μA under the rat respiration motions. The generated electricity successfully operated a pacemaker to control the heartbeat rate. Reproduced with permission.[46] Copyright 2017, John Wiley & Sons.

encapsulated with a flexible polymer to isolate it from the surrounding biofluids and to improve its robustness. The SWG was applied on a Spague–Dawley rat. After anesthesia, the rat's abdominal cavity was opened and the ventral side of the diaphragm received an SWG implantation. The deformation of the SWG caused by the mechanical vibration of normal breathing was successfully converted into electricity. The open-circuit voltage (V_{OC}) and short-circuit current (I_{SC}) outputs reached 3 mV and 30 pA, respectively.

In 2014, Hwang et al. fabricated a flexible piezoelectric NG using single crystalline 0.72 $Pb(Mg_{1/3}Nb_{2/3})O_3$–0.28 $PbTiO_3$ (PMN–PT) thin film (Figure 4B).[43] The PMN–PT ingot was grown directly from the melt by a modified Bridgman method, and poled by applying an electric field of 1.8 kV mm^{-1} for 1 h. The PMN–PT was then deposited by Au on both sides and made into a metal–insulator–metal (MIM) structure, with a total thickness of 8.6 μm. The MIM PMN–PT was transferred onto polyurethane-coated polyethylene terephthalate (PET) substrate. With an area of 1.7 cm × 1.7 cm, the maximum V_{OC} and I_{SC} of the PMN–PT NG reached 8.2 V and 145 μA, respectively, under the regular bending and release from a mechanical machine. The AC signals of the NG were converted into DC signals by doing full-wave bridge rectification using four diodes. The rectified maximum outputs were measured to be about 100 μA and 8 V respectively, which were able to operate a cardiac pacemaker that works at an input of 100 μA and 3 V.[44] The rectified outputs were directly applied to stimulate the heart of an anesthetized rat. When the PMN–PT thin-film NG was bent and released periodically, the corresponding spike peaks were observed besides the natural heartbeat curves in the electrocardiogram (ECG). Dagdeviren et al. also developed piezoelectric NG based on lead zirconate titanate (PZT).[45] The PZT energy-harvesting device was very conformal, and attached well to the heart, lung, and diaphragm, collecting the natural contractile and relaxation motions of these organs for the operation of a pacemaker.

In 2014, Zheng et al. fabricated an implantable triboelectric nanogenerator (iTENG), and for the first time, demonstrated an in vivo application of the TENG for harvesting tiny mechanical energy inside a living animal.[46] Basically, a 100 μm thick polydimethylsiloxane (PDMS) film with patterned pyramid arrays on the surface was placed on a 30 μm thick Kapton substrate, which serves as one of the triboelectric layer. Au was deposited on the other side of the Kapton film to serve as the electrode. The thin layer of PDMS and Kapton was very flexible and deformed easily in response to the slight in vivo motions of the breathing. Aluminum (Al) foil also fabricated with nanostructure modification served as both the other triboelectric layer and electrode of the iTENG. The two triboelectric layers were separated by a flexible PET spacer with a thickness of 400 μm, and they were fully encapsulated by PDMS with a thickness of 50 μm. The working area of the iTENG was only 0.8 cm × 0.8 cm, and the overall size was 1.2 cm × 1.2 cm × 0.2 cm. The output V_{OC} and I_{SC} reached about 12 V and 0.25 μA, respectively, with a power density of up to 8.44 mW m^{-2}. The iTENG was implanted under the left chest skin of a rat. The inhalation and exhalation of the rat resulted in periodic contact and separation of the thin Kapton and Al film, which in turn resulted in electricity generation. The magnitude of the in vivo generated electricity reached 3.73 V and 0.14 μA, respectively (Figure 4C). The frequency of the voltage and current peaks was consistent with the breathing rate controlled by a respirator, which was about 50 times per minute. The electricity from iTENG was stored in a capacitor and then applied to operate a pacemaker for the regulation of the heart rate. Under different working frequencies of 2, 3, and 5 Hz used, the heart rate was all successfully modulated to synchronize with the respective frequency of the pacemaker.

3.2. Cardiac Sensor

NG have not only been employed to supply energy for cardiac pacemakers, but also been applied to work as a self-powered cardiac sensor. They were implanted in the heart to directly report its beating conditions, without the requirement of any other energy supply. Implantable cardiac sensors could identify many potential arrhythmic symptoms and give out warnings or feedbacks in time.[47] Compared to wearable biomedical monitoring systems, implantable sensors could bring in continuous monitoring with higher fidelity and accuracy, casting away the limitations and artifacts caused by the patient's movement and activities.[48] With no requirement of an external power supply, NG as self-powered cardiac sensors hold great potential in the future of the healthcare industry.

Zheng et al. designed an implantable TENG (iTENG) in 2016 which enables high-output and robust operation as an in vivo cardiac sensor.[49] It was composed of core/ shell/ shell package, "keel structure," electrode layers, and triboelectric layers (**Figure 5**A). Nanostructured polytetrafluoroethylene (n-PTFE) thin film was employed as the triboelectric layer, and a Kapton film, the flexible substrate with copper (Cu) deposited on its back, served as one electrode. Al foil served as both the other triboelectric layer and the other electrode. A highly resilient titanium strip was included as the keel structure, which effectively guaranteed the contact and separation process of the n-PTFE and Al films. PDMS and Parylene were used sequentially to encapsulate the device to increase the in vivo reliability of the iTENG and avoid potential erosion by the physiological environment. Before encapsulation, the V_{OC} was about 90 V and the I_{SC} was about 12 μA; after encapsulation, the V_{OC} and I_{SC} were 45 V and 7.5 μA, respectively. The highest power density reached 107 mW m^{-2}. The iTENG was implanted between the heart and pericardium of a 30 kg male adult Yorkshire porcine. When the Kapton side was placed next to the inferior wall of the left ventricle, the in vivo V_{OC} and I_{SC} reached up to 14 V and 5 μA, which were the highest among the test positions including the outflow tract of the right ventricular, the auricle of the left atrium, the cardiac base, the lateral wall of the left ventricular, and the inferior wall of the left ventricular. The peak waves of voltage output were highly synchronous to the corresponding *R* waves in ECGs, and the correlation was calculated to be $R^2 = 0.983$. The intensity of the signals was closely related to the strength of heart beating, as demonstrated by administrating the medication epinephrine. The energy harvested by the iTENG was stored in a capacitor through a rectifier to drive a wireless transmitter, which transferred the output signals to the receiving end. In this way, the self-powered cardiac sensor with a wireless transmit system was successfully built. The whole system worked well 72 h after the closure of the chest, and was still intact and biocompatible after 2 weeks.

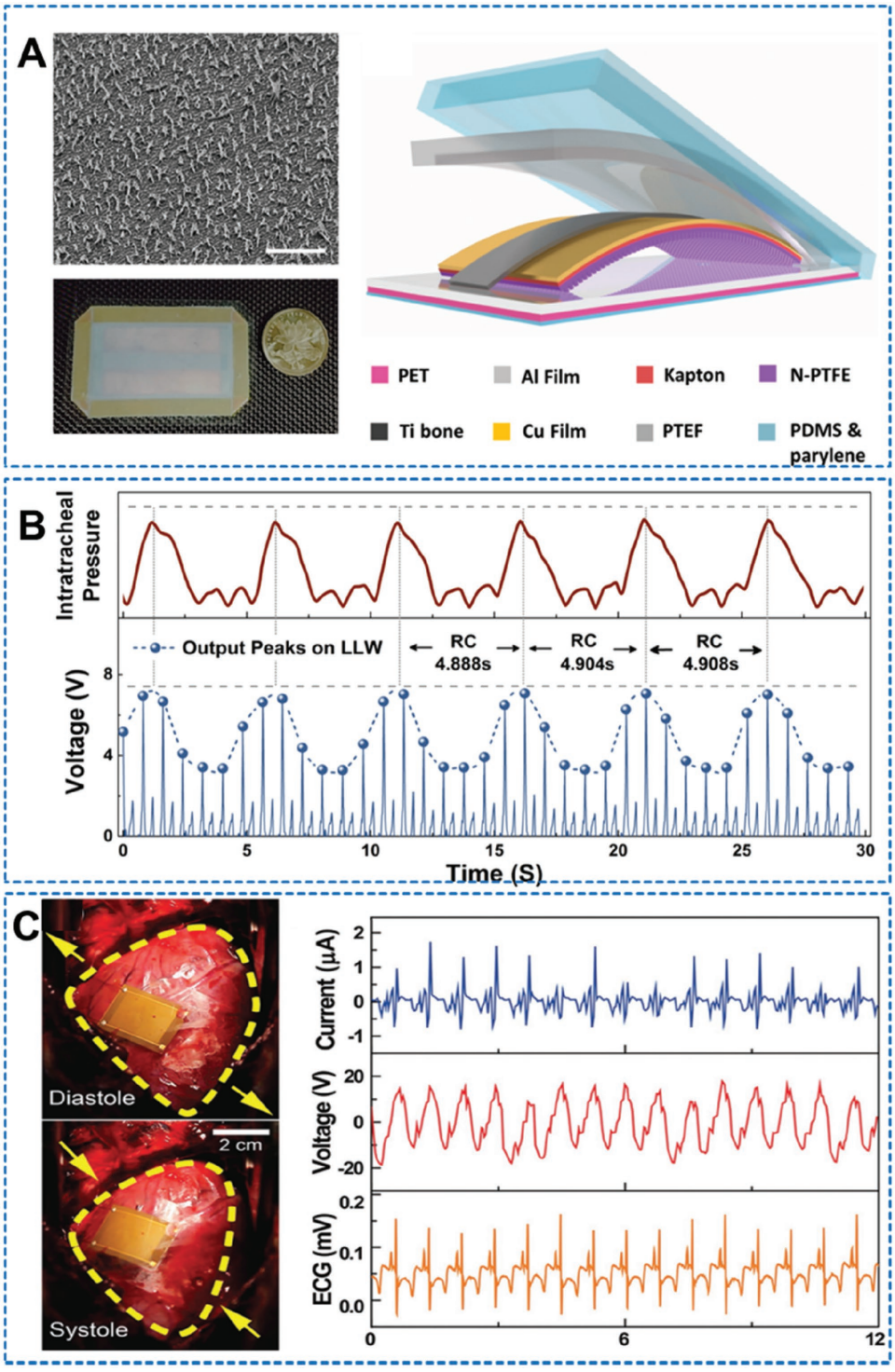

Figure 5. Various NG that have been applied as cardiac sensors. A) The schematic diagram and actual object of the TENG that worked as the cardiac sensor. Reproduced with permission.[49] Copyright 2017, American Chemical Society. B) The peaks of the output voltage form in fluctuations that were highly synchronic with the waveform of the respiration. Reproduced with permission.[48] Copyright 2017, American Chemical Society. C) The PENG cardiac sensor with the output voltage and current. Reproduced with permission.[50] Copyright 2017, John Wiley & Sons.

Ma et al. adopted the above design of NG, and obtained many more specific information of heart and blood vessel using the self-powered and one-stop implantable triboelectric active sensor (iTEAS).[48] The iTEAS was implanted between the epicardium and pericardium of a porcine and fixed to the pericardium by stitch. With the total size being $30 \times 20 \times 1$ mm^3, an electric output with a V_{OC} of about 10 V and I_{SC} of about 4 μA was yielded by the iTEAS. These electrical signals were highly synchronized with the heart

rate, reaching an accuracy of about 99%. In addition, the output signals were also highly related to the respiratory rate (Figure 5B). During the respiration, the peaks of each heartbeat-induced voltage signal fluctuated in a cyclic manner. The peaks values increased from ≈4.8 to ≈6.3 V during the process of inhalation (2.9 s) and decreased to about 3.8 V during the process of exhalation (2.0 s). The highest peak to highest peak interval was about 4.9 s, which was consistent to the ventilating rate of 12 cycles per minute controlled by the artificial respirator. Two weeks after implantation, the porcine was anesthetized for examination. The encapsulation kept the device intact, without any corrosion or rupture. The myocardium tissues were examined by hematoxylin and eosin staining, and no detectable infiltration of lymphocytes was found compared to the control tissue. These results guaranteed the promising application of NG to do the self-powered cardiac sensor task.

Kim et al. fabricated a flexible single-crystalline 0.4 $Pb(Mg_{1/3}Nb_{2/3})O_3$–0.6 $Pb(Zr,Ti)O_3$ with 0.5 mol% Mn-doped (PMN–PZT–Mn) piezoelectric NG as a self-powered cardiac sensor.[50] After sternotomy, the PMN–PZT–Mn thin-film device was sutured onto the epicardium of a porcine by doing one stitch at each corner to get conformal contact. The bending stiffness of the device was 9.95×10^{-5} N m, smaller than that of the medical patch for cardiac surgery (2.52×10^{-3} N m); therefore, it did not affect the physiological activity of the heart. Driven by the contraction and relaxation of a porcine heart, the single-crystalline flexible energy harvester generated a V_{OC} of 17.8 V and an I_{SC} of 1.75 µA (Figure 5C). The peaks of V_{OC} and I_{SC} correlated well with the R peaks of the ECG curves in response to various heartbeat frequencies (1.7, 2.7, and 5.3 Hz). The output signals were remained stable without performance degradation during 100 000 cycles of bending and releasing. The device was very compatible for biomedical application, as demonstrated by cell viability assay using HEK293, H9C2, and HL-1, as well as the histological staining of the surrounding tissues. In 2017, Jeong et al. fabricated a new $LiNbO_3$-doped (K, Na)NbO_3 thin-film based piezoelectric NG containing no lead element, which demonstrated excellent biocompatibility and very high output.[33]

3.3. Blood Pressure Sensor

Hypertension, or high blood pressure (BP), is a long-term medical condition, and also a very important risk factor for heart failure and cerebrovascular diseases.[51] About 51% of cerebrovascular disease and 45% of ischemic heart disease globally are related to hypertension.[52] Due to the aging of population, the burden of hypertension is increasing year by year. An implantable blood pressure monitor could play an important role in early diagnosis and accurate assessment of disease and drug, which will consequently reduce the cost of healthcare.[53,54] Here again, a self-powered BP sensor would be of great advantage because it can avoid the problem of energy depletion.

To use the pulsation of aorta directly as a power source for the BP sensor is an appealing approach. However, due to the brittle feature of aorta and the extremely limited space of the organ in vivo, the device is required to be very thin, flexible, and stable.[55] A series of research have been carried out to develop piezoelectric polymer-based thin-film NG to be the BP sensor.[56,57] In the most recent work, the sensor was fabricated with a 200 µm piezoelectric thin film of polarized PVDF in a sandwich structure with thin Al layers as the electrodes (**Figure 6**).[57] The whole structures were encapsulated by 50 µm polyimide films. The

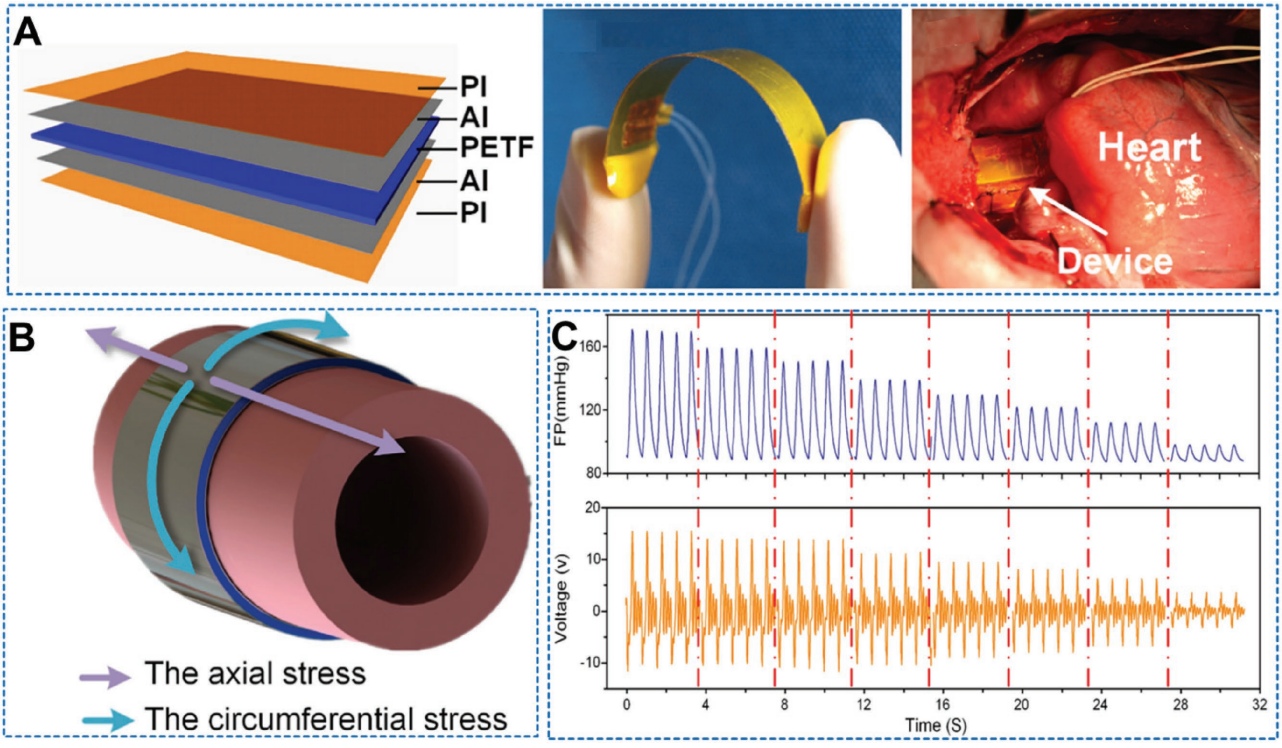

Figure 6. A) The flexible and thin PENG can be wrapped around B) the aorta and work as the C) in vivo self-powered BP sensor. Reproduced with permission.[55] Copyright 2017, Elsevier.

Young's modulus of the device was 3500 MPa, pliable enough to be applied on the aorta. Once wrapped on the aorta, periodic voltage and current are formed with the expansion and retraction of the aorta. When tested on an in vitro model of aorta pulsation with a balloon pump and a latex tube filled with saline, a high linearity ($R^2 > 0.99$) with a sensitivity of 173 mV mmHg^{-1} was obtained in this PVDF-based BP sensor. A maximum instantaneous power of 2.3 μW was reached. When wrapped on the ascending aorta of a male Yorkshire porcine of more than 50 kg, a favorable linearity ($R^2 > 0.971$) with a sensitivity of 14.32 mV mmHg^{-1} was obtained, and the device output has a maximal instantaneous power of 40 nW in vivo. The positive and negative voltage outputs correlated with the systolic and diastolic phases of the BP. Excellent stability of the device was also achieved for more than 50 000 operating cycles. An liquid crystal display (LCD) was integrated in the circuit and placed on thoracic skin of the animal. When the voltage of the PVDF device, as a sensor and a power supplier, was higher than 2 V, which meant that the systolic BP was higher than 140 mmHg, the LCD would be turned on to warn of this situation. In this way, a self-powered BP monitoring system was built.

3.4. Pulse Sensor

Real-time biomedical monitoring systems have resulted in a tremendous medical breakthrough in the modern lifestyle because they can build bilateral and instantaneous communications of physiological signals and help to make automatic medical diagnosis. While implantable devices can provide un-substitutable advantages for inner-body signal transmission, wearable devices are more adoptable if they can detect the body signals at equivalent sensitivity and accuracy. The pulse sensor is an appealing approach to investigate and monitor the circulatory system, because the pulse is closely related to the heart and aorta. A self-powered pulse sensor has an even more exciting solution, because the avoidance of battery can reduce the energy consumption and environmental pollution, miniaturize the device size, and increase the signal fidelity.

Park et al. in 2017 produced an ultrathin and conformal piezoelectric sensor based on PZT.[58] A high-quality PZT thin film was coated and annealed on a sapphire substrate, then the PZT thin film was exfoliated and transferred to an ultrathin PET substrate (a thickness of 4.8 μm) using a UV-cured adhesive polymer. Gold-interdigitated electrodes were formed on the PZT thin film. The device was thin enough to float on soap bubbles (**Figure 7**A). Then the piezoelectric sensor was conformally attached to a human wrist with the help of liquid bandage. The real-time pulse signals were transferred through wireless transmission to a smart phone to do pulse monitoring. The sensor was applied on a young man of about 30 years old. The NG and senor generated a V_{OC} of 400 mV from the carotid artery pulse and 100 mV from saliva swallowing action. The output voltage measured by the carotid artery is roughly six times higher than that by radial artery due to high carotid artery blood pressure. The radial artery pulse generated an average V_{OC} of 65 mV and 73 beats per minute (BPM) before exercise, and a V_{OC} of 81.5 mV and 100 BPM after exercise, respectively. In each cycle of the voltage signals, there were two peaks, P1, and P2, which meant the sum of the forward travelling wave and reflected wave, and the reflected wave from the lower body subtracted by the end-diastolic pressure, respectively.[59] The radial artery augmentation index (AI_r), defined as P2/P1, is strongly related to arterial stiffness. Before exercise, the sensor reported average values of AIr to be 0.54, and after the exercise, the average value of AIr was found to be 0.22. This suggested a decrease in the late systolic augmentation, most possibly due to the changed heart rate, enlarged ventricular ejection, or artery stiffness after exercise.

Ouyang et al. in 2017 fabricated a triboelectric NG-based self-powered ultrasensitive pulse sensor (SUPS) with high flexibility and excellent output performance.[60] Nanostructured Kapton and Cu thin films were employed as the two triboelectric layers. After being encapsulated by PDMS, the entire device had a dimension of 20 mm × 10 mm × 0.1 mm, which was very thin and flexible. At the drive of a linear motor with a vertically compressive force of about 50 N, the output voltage, current, and transferred charge of the SUPS were up to 109 V, 2.73 μA, and 7.6 nC, respectively. When applied on the radial arteria of a 24 year old man, the outputs of the SUPS were 1.52 V, 5.4 nA, and 1.08 nC, respectively. The peak waves of the SUPS voltage output were synchronous to the corresponding *R* waves in the ECG, with a linearity of $R^2 = 0.981$, which was higher than other clinically adopted pulse sensors, piezoelectric pulse transducer (PPT) and photoplethysmography (PPG) (Figure 7B). The ability of SUPS to diagnose cardiovascular diseases and antidiastole was investigated in several groups of patients. The groups are healthy group, coronary heart disease (CHD) group, atrial fibrillation (AF) group, and atrial septal defect (ASD) group. There were obvious differences between the voltage waveforms of the healthy and unhealthy groups. The time intervals of $P - P_n$ and $P - P_{n+1}$ were presented in Poincare plot, and each group showed their specific pattern (Figure 7C). The healthy group presented a comet-shaped plot. The CHD group showed a plot with several small disperse comets. The ASD group showed an ellipse plot with relatively even distribution. The AF group showed largely scattered distribution. The obvious difference of Poincare plot between the healthy people and patient groups enabled SUPS to be a useful tool in the antidiastole of cardiovascular illness. Many other indicators were calculated according to the time domain of the output waveforms of SUPS, including the standard deviations of all normal sinus *R*–*R* intervals for all 5 min segments, the root-mean-square value of successive normal sinus *R*–*R* interval difference, the percentage of successive normal sinus *R*–*R* intervals >50 ms (PNN50), the artery stiffness (SI), and the aortic augmentation index (AIx). The difference between each group was consistent with previous studies.[61,62] Last but not the least, because SUPS had high resolution of time, it showed superiority in measuring the pulse wave velocity (PWV). Two sensors 4.5 cm apart were placed on the radial artery of the wrist. Before and after the exercise, the PWV increased from 8.92 to 10.83 m s^{-1}. The high sensitivity suggested that SUPS could be well applied in an intelligent mobile diagnosis system.

4. NG Application in the Neural System

4.1. Deep Brain Stimulation

Deep brain stimulation (DBS) is a neurosurgical procedure to stimulate a specific brain area with electric pulses for treatment

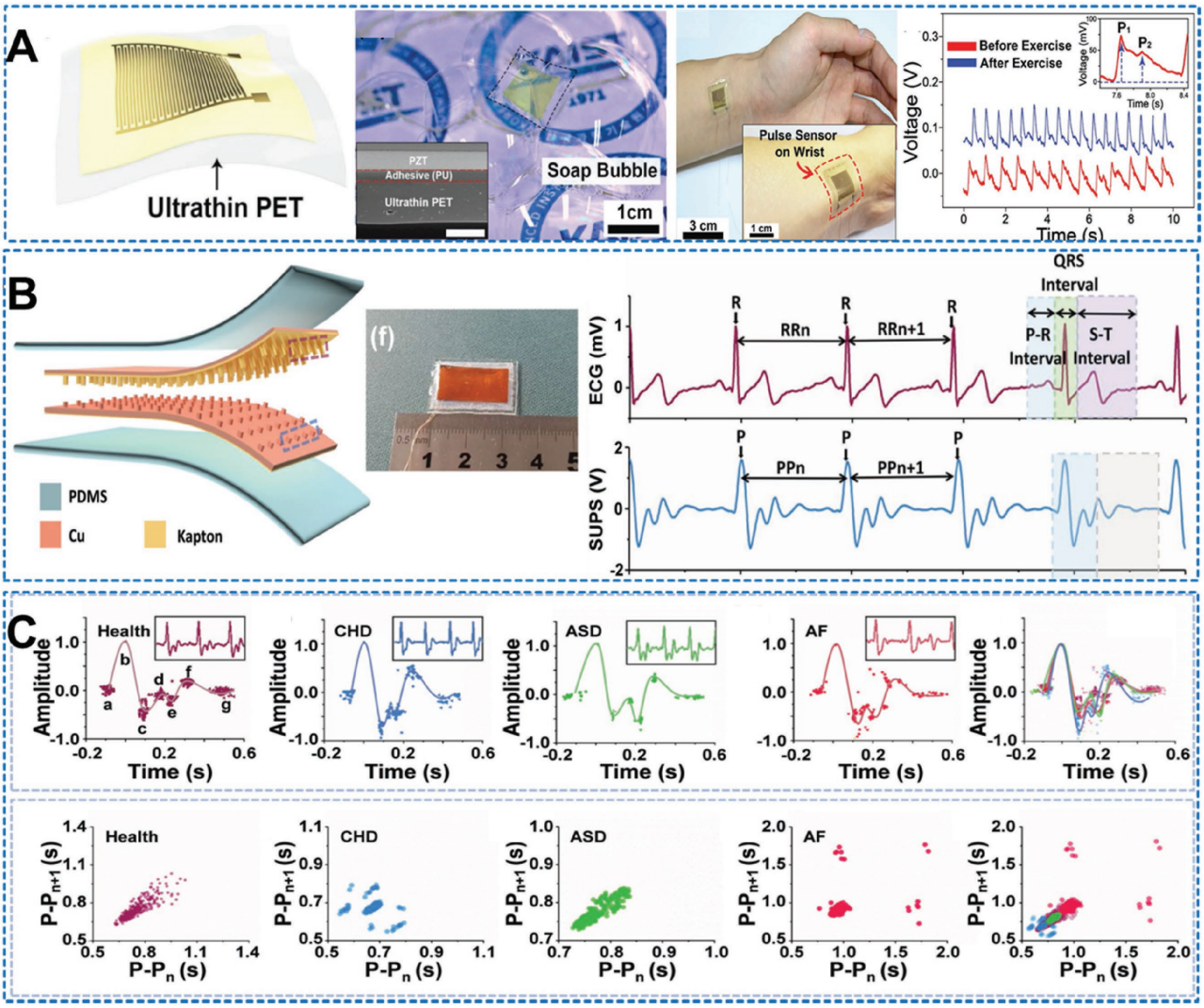

Figure 7. The NG can be employed to be wearable pulse sensors. A) The ultrathin and flexible PENG pulse sensor and the output voltage signal. Reproduced with permission.[58] Copyright 2017, John Wiley & Sons. B) The TENG pulse sensor and the output voltage signal; the peak of the voltage waveform was highly coordinated with the peaks of the ECG waveform. Reproduced with permission.[60] Copyright 2017, John Wiley & Sons. C) The TENG sensor signals demonstrated different patterns for patients from different disease groups. Reproduced with permission.[60] Copyright 2017, John Wiley & Sons.

purpose.[55] It has been proved to be effective in alleviating various symptoms of neurologic and psychiatric disorders, including epilepsy, Parkinson's disease, essential tremor, and major depression.[63,64] An implantable brain stimulator requires high operation power, operating at 3–5 V, 130 Hz, with a pulse duration of 60 ms, which are several folds higher than an artificial cardiac pacemaker (2 V, 1 Hz, with a pulse duration of 400 ms). To accomplish a self-powered strategy for DBS, larger challenges of the design, fabrication, and implantation of the NG are raised.

Kim and co-workers fabricated a flexible single crystalline $Pb(In_{1/2}Nb_{1/2})O_3$–$Pb(Mg_{1/3}Nb_{2/3})O_3$– $PbTiO_3$ (PIN–PMN–PT: PIMNT) film on a plastic PET substrate and tried out its applications in the DBS approach in 2015.[65] The PIMNT film was made as thin as 10 µm, and the PET substrate was 125 µm, which together made an ultrathin device (**Figure 8**A). Under the bending of a mechanical machine, the maximum open-circuit voltage and short-circuit current were 11 V and 283 µA, respectively, which could charge capacitors and turn on 120 green light-emitting diodes. Under the bending of human fingers, the PIMNT NG generated a highest current of 0.57 mA and a power of 0.7 mW. This PIMNT-based DBS was applied to activate the primary motor (M1) cortex in a live mouse brain. The generated electric energy was directly transmitted to the stimulation electrode via metal wires, and the stimulation electrode was placed at the accurate position of the M1 cortex of the mouse. Each bending cycle of the PIMNT NG resulted in a contraction of the forelimb muscle and 1.5–2.3 mm displacements of the right paw. This work is an important step forward the self-powered direct DBS by a body-motion-driven NG.

4.2. Nerve Stimulation

After spine cord injury, the neural signal transmissions from the brain to the muscles get greatly interfered. Functional electrical

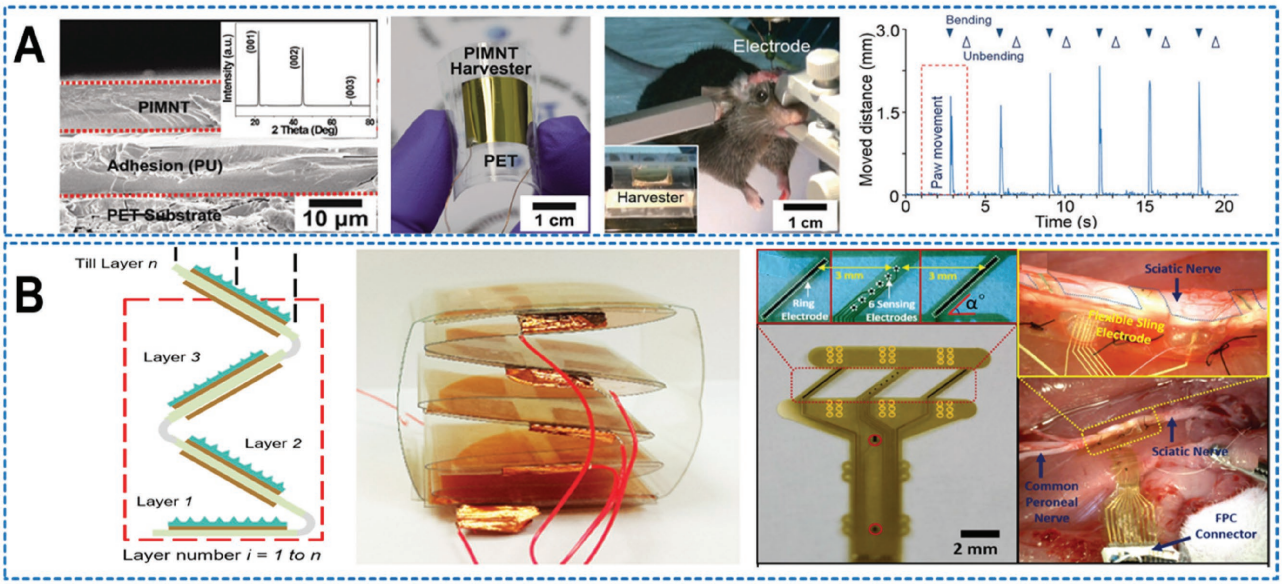

Figure 8. The fabricated NG for in vivo neural system stimulation. A) The output of the PIMNT-based NG was applied on the M1 cortex of a mouse brain, and the mouse paw made displacement in accordance with the NG output. Reproduced with permission.[65] Copyright 2017, Royal Society of Chemistry. B), the Zigzag NG was connected to the flexible neural interface to do nerve stimulation. Reproduced with permission.[67] Copyright 2017, Elesvier.

stimulation is employed to apply low-energy electrical pulses to artificially enable muscle contraction and body movements in the patients who have been injured in the central nervous system. The electrical stimulation can be applied on either the downstream motor neurons or the target muscles to active the muscle and restore some part of control over the abnormal body.[66]

Lee et al. developed[67] a zigzag-shaped TENG with several units stacked together. A PET sheet was used for mechanical support. Cu and PDMS films with nanopatterns were employed as the contact layers. During the compress and recover of the zigzag structure, the Cu films got contacted with two pieces of the PDMS layers (Figure 8B). With a configuration of five units in parallel, the TENG generated a V_{OC} of about 68 V, an I_{SC} of about 1.9 μA, and a maximum power of 51.8 μW. The neural stimulation electrodes were fabricated with two layers of flexible polyimide with gold sandwiched between. The output of the TENG under the drive of human hand tapping was applied through the flexible stimulation electrodes onto the sciatic nerve of a rat. The electrical simulation resulted in the contraction of tibialis anterior (TA) and gastrocnemius medialis (GM) muscles, leading to the twist of the leg. The recorded electromyogram of the TA and GM muscles showed that the frequency of the muscle electric potential conformed well to the stimulation current of the TENG.

5. NG Application in Cell Modulation

5.1. Neuronal Cells' Differentiation

Injuries in the nervous system often result in poor prognosis, which have caused severe burdens to the patients and their family.[68] Neural tissue engineering (NTE) is believed to be a promising approach to promote regeneration of neural systems,[55] which is composed of therapeutic neural cell, scaffold, and bio/chemical/physical cues.[69] Mesenchymal stem cells (MSCs) are the most abundant and available therapeutic stem cell sources for NTE.[70] In this circumstance, efficient methods to induce MSCs differentiate into neural cells are crucial to do NTE. Meanwhile, direct reprogramming of somatic cells to therapeutic neural cells is another appealing strategy for treating neuronal disorders, because it avoids the ethical issues associated with the use of human embryos and reduces the risk of tumorigenesis associated with the use of pluripotent stem cells.[71]

Guo et al. in 2016 combined a small-sized TENG and conductivity-improved microfibers to enhance MSC neural differentiation.[72] Polymethyl methacrylate (PMMA) and Al were chosen as the friction materials. The two friction layers were connected and separated by four springs at the corners. Copper layers were laminated in the outer sides of PMMA and Al as electrodes (**Figure 9**A). When triggered by a motor with a displacement of 0.5 mm and a frequency of 1.4 Hz, the TENG generated a V_{OC} of about 300 V, an I_{SC} of about 30 μA, and a transferred charge of about 18 nC. When driven by human stepping, the TENG generated very close outputs to that of the motor, which were applied on microfibers as the neural scaffold. The microfibers were made from reduced graphene oxide (rGO), with poly(3,4-ethylenedioxythiophene) (PEDOT), added to improve the electrical conductivity, which was increased from 1.51 to 2.52 S cm^{-1} after 15% PEDOT doping. Both rGO and rGO–PEDOT microfibers showed excellent biocompatibility to maintain cell viability. TENG electrical stimulation was applied on the rGO and 15% rGO–PEDOT microfibers for 21 d. The expression of Tuj1 (marker gene for neuron lineage) and GFAP (marker gene for glial lineage) was assessed. Without the TENG stimulation, MSCs cultured on both microfibers showed no expression of Tuj1 and GFAP. With the TENG stimulation, MSCs cultured on both microfibers showed distinct expression of the two genes. In addition, the expression

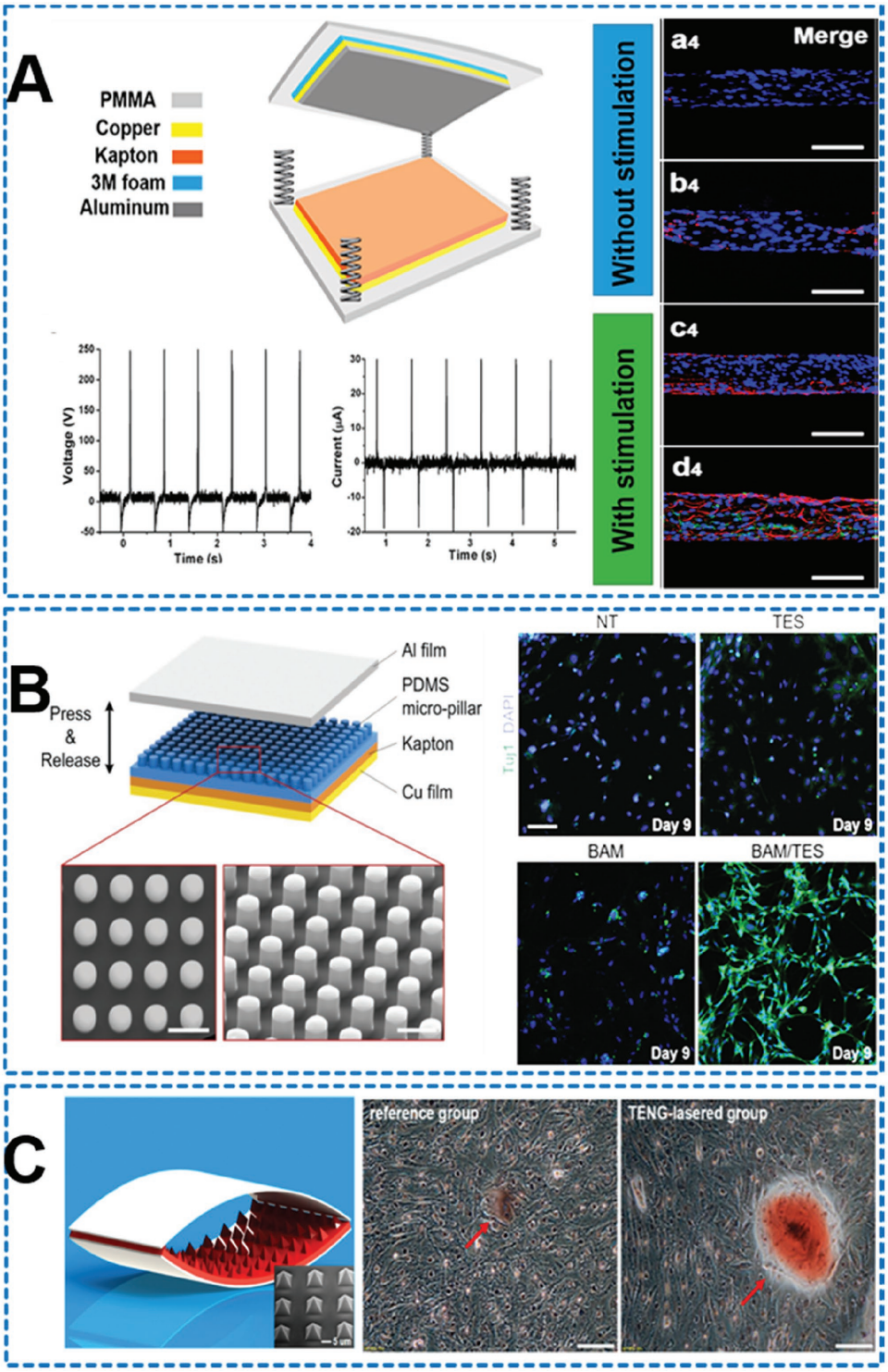

Figure 9. The application of NG for cell differentiation enhancement. A) The MSC growing on the conductive fibers presented much more Tuj1 (green fluorescence) and GFAP (red fluorescence) expression with the TENG stimulation. Reproduced with permission.[72] Copyright 2017, American Chemical Society. B) The Tuj1 (green fluorescence) expression of the fibroblast cells with only plasmid or TENG treatment, and with both treatment. Reproduced with permission.[73] Copyright 2017, John Wiley & Sons. C) The TENG increased the differentiation of MSC to osteoblast cells. Reproduced with permission.[77] Copyright 2017, American Chemical Society.

of Tuj1 on the 15% rGO–PEDOT was enhanced by ≈1.68-fold over that on the rGO microfiber, and that of GFAP was enhanced by ≈1.5-fold.

Jin et al. in 2016 tried out the strategy of using a triboelectrical stimulator (TES) to assist the direct reprogramming of fibroblast cells into neural cells by transcription factors'

(TFs) transfection.[73] The triboelectric layers were consisted of aluminum (Al) and PDMS, respectively. The PDMS layer was made with micropillar structure glued to a Kapton film, which was attached to a Cu electrode (Figure 9B). The output voltage and current from TES reached a V_{OC} of about 30 V and an I_{SC} of about 280 nA under the periodic force of a mechanical machine. The output was transmitted by metal wires to the cell culture substrate which had been deposited with a Ti layer. The fibroblast cells were cultured on the Ti-coated culture template with the TF-expressing plasmids,[74] and received TES every day at 60 min per day for a frequency of 1 Hz. The efficiency of generating neural cells by transfecting the TF-expressing plasmids alone was 6.41%, which was increased to 14.17% with the assistance of TES, and increased neurite extension was observed in the TES group. This is the highest efficiency ever reported to induce Tuj1-positive neural cells by the nonviral gene delivery method.[70] The mechanism was speculated to be the elevated intracellular Ca^{2+} levels after exposure to TES. Ca^{2+} ions play a vital role in neuronal development and regulation, which may activate ERK1/2 signaling pathway and protein kinase C as an early response, resulting in the induction of genes involved in various cellular functions and cell maturation.[70] This study showed the possibility of doing nonviral in vivo neuronal reprogramming by TF-expressing plasmid injection with the assistance of a self-powered implantable TES system.

5.2. Osteoblast Cells' Differentiation

After bone injury, how to accelerate the long-term bone regeneration process is a fundamental issue.[75] Recently, it has been recognized that low-level laser therapy has a positive effect on the healing process possibly because the laser energy corresponds to the characteristic energy and absorption levels of the respiratory chain in mitochondria.[76] To adopt this technology, an implantable laser cure system is required. A self-powered, implantable power source could realize an integrated all-in-one system without battery limitation.

Tang et al. in 2015 tried out this strategy and developed a self-powered low-level laser cure system for osteogenesis based on a TENG and infrared laser excitation units.[77] This system significantly accelerated the mouse embryonic osteoblasts' proliferation and differentiation. Pyramid array patterned PDMS and indium–tin oxide (ITO) films were utilized as the friction materials (Figure 9C). The TENG output has an I_{SC} of about 30 μA and a V_{OC} of 115 V, with the transferred charge per cycle being about 70 nC. MC-3T3 osteoblast cells were set into three groups: reference group with no laser treatment, laser-irradiated group driven by TENG (TENG-laser group, 100 pulses per day);), laser-irradiated group using a battery (battery-laser group, 1 min per day). The cells proliferation increased by about 15% in laser irradiation groups. After 5 d, the differentiation level in the TENG-laser group was increased by 16.9% compared to the reference group, while the battery-laser group increased by 21.7%. This equivalent improvement verified the application of TENGs to be the energy source for implantable medical devices for clinical therapy of bone remodeling and healing.

6. NG Application in Microbe Disinfection

The shortage of clean water is one of the worldwide problems that impair people's quality of life. Water contamination is prevalently caused by microbe pathogens that may lead to infectious epidemic diseases such as diarrhea.[78] Another severe threat to clean water is caused by human "invasion," that the industrial discharge and runoff from farms resulted in extra nutrients in the water.[79] The algal blooms will cause depletion of the dissolved oxygen in water and suffocate other aquatic life, causing ecological disasters.[80]

6.1. Microbe Inactivation by Electroporation

High electric field sterilization has been widely used in rapid disinfection of food and milk. It requires very short treatment time and produces no by-products. When the electrical field (EF) exceeds 10^6 V m^{-1}, irreversible electroporation and membranes disruption will occur in living cells including bacteria. To reduce the cost of producing very high voltage, nanostructure electrodes are introduced, which can generate EF larger than 10^6 V m^{-1} at their surrounding area at voltages of less than 100 V.[79,81] This microbe disinfection technology has been combined well with NG to make self-powered water decontamination.

Jiang et al. in 2015 reported a self-powered electrochemical water treatment system for sterilization and algae removal in water using TENG that was driven by the power of water waves.[82] The arch-shaped TENG (15 cm × 30 cm in size) is consisted of an ITO-coated PET film with a thickness of 150 mm as the top plate and a PET–ITO–PTFE film as the bottom plate, with the triboelectric layers being ITO and PTFE. A total of 50 TENGs in parallel were placed inside a swimming pool, and driven by repetitive emerging–submerging water waves (**Figure 10**A). Each TENG generated a V_{OC} of about 270 V and an I_{SC} of about 120 μA. The output after rectification was delivered to mixed metal oxides (MMO)–Ti–rGO electrode plates, which were made of MMO–Ti plates electrodeposited with rGO on the surface. The distance between cathode and anode was set as 2 cm. This system achieves more than a 6 log (99.9999%) removal of three model bacteria, and high removal efficiencies for mixed marine algae. Apart from electroporation, the synergetic effect of both free chlorine and reduced graphene oxide during the electrolysis process was also believed to play a role in the high-efficiency bacteria and algae removal.

Tian et al. in 2016 reported the killing of in-water bacteria by electroporation on the ZnO/Ag nanobrush electrodes under the electrical supply of a wave-driven TENG.[83] The TENG in this system had a ball-in-ball structure, and the triboelectric layers were consisted of a rubber ball and Al foil. They were encapsulated and supported by a plastic ball, and further encapsulated by PDMS (Figure 10B). The wave-driven TENG output has a V_{OC} of 50 V and an I_{SC} of about 2 μA. The electricity generated by the TENG was connected to two carbon-cloth-based electrodes. ZnO nanowires were allowed to grow on the cloth fibers and additionally doped by Au nanoparticles to make the nanobrush structure. During TENG

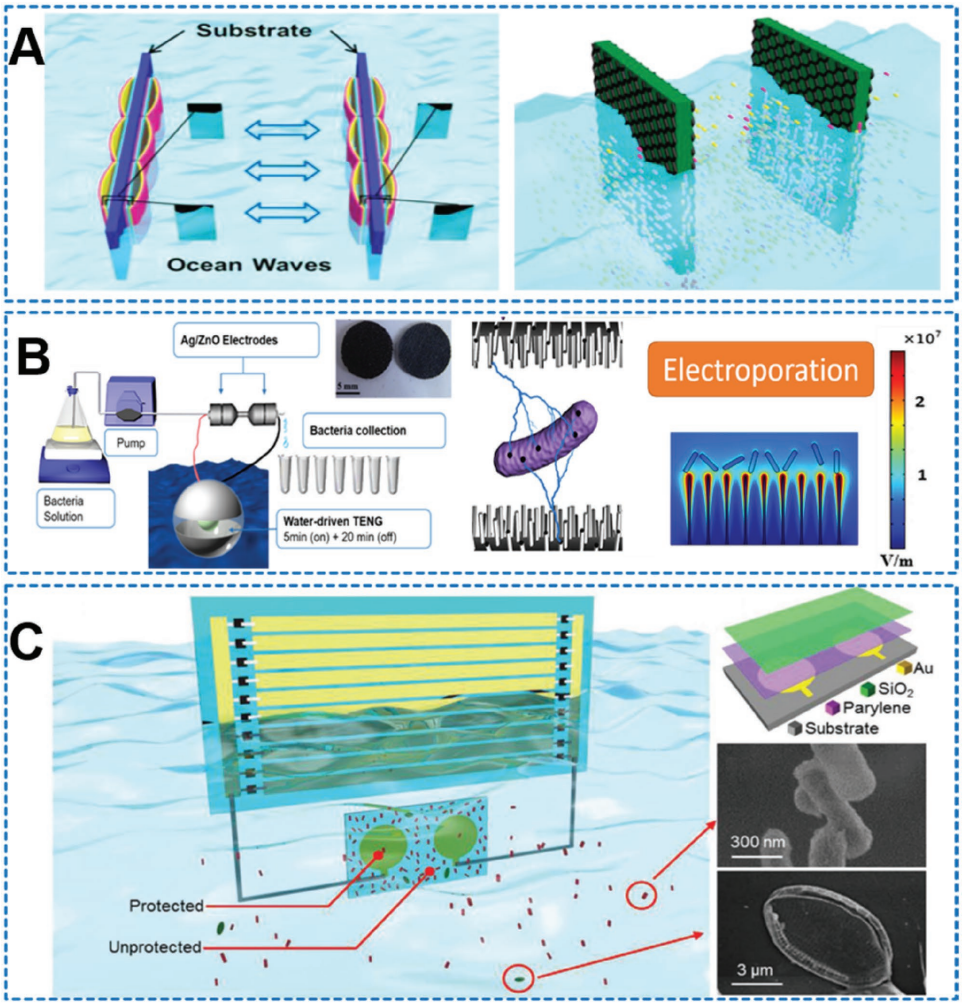

Figure 10. The water-driven NG for antibacterial application. A) The parallel ITO–PTFE TENG with Ti-rGO plate as the electrodes. Reproduced with permission.[82] Copyright 2017, Elsevier. B) The ball-in-ball TENG with Ag/ZnO nanobrush electrodes. Reproduced with permission.[83] Copyright 2017, Elsevier. C) The self-powered antibiofouling device. Reproduced with permission.[84] Copyright 2017, John Wiley & Sons.

operation, the number of colony forming units (CFU) of *Escherichia coli* decreased from 10^6 mL^{-1} to 0 within 0.5 min, achieving a complete killing. With *Staphylococcus aureus*, it resulted in more than two order of magnitude CFU reduction (sterilization rate, SR ≈ 99%). For natural river water, the SR was also about 99%. Pores and holes in the bacteria membrane were found under the scanning electronic microscopy (SEM) observation, demonstrating the killing mechanisms caused by this wave-driven system.

6.2. Antibiofouling Activity

Biofouling is the adherence of bacteria, biofilm, plants or animals on wetted surfaces.[80] It causes frustrating problems to a wide variety of industries including underwater facilities, shipping, coastal constructions, oil pipelines, and underwater sensors. High EF has been found effective in preventing biofouling. To integrate the EF prevention with wave powering would be a great step forward, because this approach can enable self-powered biofouling prevention.

Zhao et al. in 2016 developed a triboelectric wave harvester (TEWH) that demonstrated strong antibiofouling property.[84] An array of strip-shaped ITO electrodes were deposited on a flexible PET substrate. The ends of the electrodes were connected to rectifying chips, which guaranteed that electrons are always transported from the cathode to the anode. The induced charges were periodically transferred to the antiadhesion electrodes. The electric potential oscillated in the positive direction at the anode side and vice versa. The peak-to-peak value of the oscillation voltage reached up to 300 V. The circle-shaped electrodes were embedded in the underwater unit, and encapsulated by a layer of water-proof silicon dioxide. When the TEWH started working, the surface section with the circle electrodes underneath was significantly protected against microbe adhesion (Figure 10C). The antiadhesion efficiencies for *E. coli*, positive-gram bacteria *S. aureus*, and diatoms (bacillariophyceae) were as high as 99.3%, 99.1%, and 96.0%, respectively. It was speculated that the

inherent charge distribution on the microbes was disturbed by the oscillating EF due to electrostatic induction, which prohibited their initial adhesion onto the surface where EF presented.

6.3. Postcharge Disinfection

The results discussed above were all obtained when the electrical field was applied on the electrodes, which was compliant with the common understanding of bacteria killing. However, Tian et al.' in 2016[83] discovered some unexpected results, which can be described as "postcharge disinfection."

Once the ball-in-ball TENG started working and transmitted the electricity to the two parallel ZnO/Ag nanobrush electrodes, bacteria disinfection was induced not only during the TENG power supply, but also in dozens of minutes after the TENG power was turned off. Compared to ZnO nanobrush electrodes, the ZnO/Ag electrodes had larger capacitance, and also showed larger postcharge disinfection efficiency. Notably, the postcharge disinfection took place in freshly replaced solution after the charging was stopped; therefore, the disinfection was not caused by any possible electrochemical product during the charging process. In addition, if the electrodes were not charged by TENG, they only had the baseline disinfection ability. In addition, the AC output was not converted into DC outputs using a full bridge-rectifying circuit,[85] but was used directly on the ZnO/Ag electrodes. How did AC signals of the TENG influence the capacitive electrodes and result in the postcharge disinfection property? This finding added a new understanding of the AC input and capacitive materials. It also suggested a new approach for water disinfection or surface disinfection that can be still effective after the charge is turned off.

7. NG Application as Biodegradable Electronics

In modern society, implantable medical devices (IMD) have become indispensable for medical treatment, which have greatly improved people's quality of life and prolonged patients' lifespan.[86] Over decades, researchers have tried hard to solve the problems of the mismatch between the hardness of IMD and the softness of biological issues. IMD built from conformal and biodegradable materials are highly welcome and desirable.[87] Since NG have been demonstrated to be promising candidates as implantable energy suppliers, the development of biodegradable NG is imperative.

Zheng et al. developed a biodegradable TENG (BD-TENG) to harvest biomechanical energy in vivo, which was completely degraded in several months after implanted in mice (**Figure 11**A).[88] The as-fabricated BD-TENG has a multilayered structure:

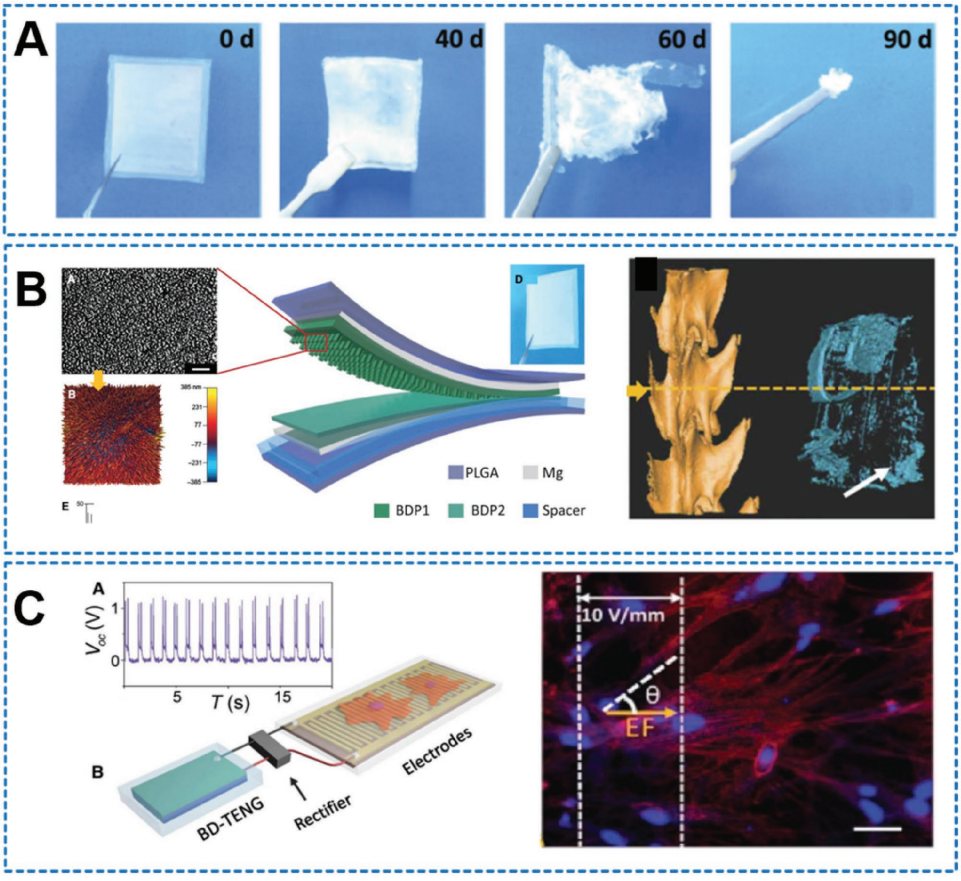

Figure 11. The biodegradable TENG. Open Access[88] A) The degradation process of the TENG in vitro. B) The schematic diagram of the TENG and its degradation in vivo. C) The application of the TENG output to modulate the neuron alignment.

the encapsulation layer (poly(lactic-co-glycolic acid) (PLGA)), the friction layers (PLGA and polycaprolactone (PCL)), the electrode layers (Mg), and the spacer (Figure 11B). The V_{OC} reached about 40 V, and the I_{SC} about 1 μA. This BD-TENG was employed to modulate nerve cell growth orientation, which was also very important for neural injury repair. Primary rat neuron cells were cultured on a Kapton substrate with Cu interdigital electrodes, which was covered by a thin PDMS film (100 mm) to avoid the electrochemical reaction on the copper electrodes. The BD-TENG with a rectified V_{OC} of 1 V was connected to the electrodes and produced an EF of 10 V mm^{-1}. Primary neurons were seeded on the stimulation device modified with polylysine and exposed to repeated electrical stimulation after 24 h culture. EF treatments of 0 (control) and 10 V mm^{-1} at 1 Hz were applied for 30 min per day. After 5 d of culturing, the nucleus and cytoskeleton revealed that most of the electrically stimulated neurons were well oriented parallel to the EF (Figure 11C), whereas those in the control group had no obvious orientation.

8. Conclusion

There are plenty of power sources in living humans and animals, in the forms of chemical, thermal, and mechanical energies.[89] Making use of these energies can help to build up self-powered healthcare electronics and benefit for the development of long-term wearable/implantable medical devices. Various strategies have been developed to harvest the different forms of energies. This review focuses on the development and application of NG, including both PENG and TENG, which have the capacity to harvest mechanical energy from the body motions of living subjects.

Many NG have been applied in many biomedical fields, including the circulatory system, neural system, stem cell differentiation, water decontamination, and biodegradable electronics. Apart from the above major applications, some other approaches are under investigation, for example, drug delivery,[90] voice recognition,[91] and bio-monitoring.[92] The development and application of these self-powered biomedical devices will exert significant impact on the healthcare industry. However, this is just the beginning of this field. To make full use of the advantages of NG-powered medical systems, more extensive and in-depth studies are inevitable. For implantable application, first, the NG should be more miniaturized, so that they can be successfully implanted in certain cavity inside the body. Second, the NG need to be more flexible and durable to match the mechanical property and the shape of the implantation spot, and endure the long-term extrusion of the muscles. In addition, more efficient, durable, and flexible encapsulation should be accomplished to protect NG from the corrosion of the body liquid. Finally, the optimization of the output performance and power management of NG need to be carefully settled to compromise with the actual operation parameters of the medical devices. For wearable NG, the issues of miniaturization, duration, encapsulation, and output performance are also very important.

The development of nanomaterials, mechanical science, and fabrication techniques have enabled the extensive studies and progress of NG in biomedical field. A prospective research direction would be to further combine the NG development more precisely with the medical principles. There are still obvious gaps between the present NG research and the actual clinical applications. First, the implantable NG as cardiac or aorta sensors have been able to work independently by themselves and realize wireless data transfer. However, the implantation of the NG to the heart or the aorta involves complicated surgery, and may hamper the normal functions of those organs. Therefore, the criteria to allow in such devices may be very high, leading to rear application of these NG sensors. Second, the integration of body-driven NG with the power management system is another challenge, because only the electrical stimulations of some specific parameters can play the role of enhancing organ healing, modulation, or generation. Third, many experiments have been carried out in vivo using NG, either employing the natural muscle contractions to generate electricity or receiving the electrical stimulation produced by an external NG driven by linear motor or intended hand tapping. However, up till now it is still hard to approach an integrated all-in-one system with power generation and management, automatic control, and stimulation system working as a whole in vivo. Nevertheless, the progress of NG in the biomedical field would definitely open new routes for the development of healthcare electronics. In our opinion, one of the most promising application perspectives for NG as implantable devices could be harvesting the energy of the breath cycle, that is, the regular expansion movement of the chest during respiration, to provide electrical supply for cardiac pacemakers or spinal injury repairs. As for wearable NG devices, working as pulse sensor is definitely an appropriate and attractive approach. They could also work well to provide electrical stimulation for some superficial treatment, for example, the wound healing or superficial tumor ablation.

Acknowledgements

H.Q.F. and C.C.Z. contributed equally to this work. This work was supported by the national key R&D project from Minister of Science and Technology, China (2016YFA0202703), National Natural Science Foundation of China (Grant Nos. 31571006, 81601629, and 61501039), Beijing Natural Science Foundation (Grant No. 2162017), Beijing Talents Fund (2015000021223ZK21) and "Thousands Talents" program for pioneer researcher and his innovation team.

Conflict of Interest

The authors declare no conflict of interest.

Keywords

biomedical applications, healthcare electronics, nanogenerator, self-powered system

Received: November 8, 2017
Revised: December 9, 2017
Published online:

[1] G. T. Hwang, M. Byun, C. K. Jeong, K. J. Lee, *Adv. Healthcare Mater.* **2015**, *4*, 646.
[2] R. Hinchet, S. W. Kim, *ACS Nano* **2015**, *9*, 7742.
[3] A. Proto, M. Penhaker, S. Conforto, M. Schmid, *Trends Biotechnol.* **2017**, *35*, 610.
[4] Q. Zheng, B. Shi, Z. Li, Z. L. Wang, *Adv. Sci.* **2017**, *4*, 1.
[5] M. Yuan, L. Cheng, Q. Xu, W. Wu, S. Bai, L. Gu, Z. Wang, J. Lu, H. Li, Y. Qin, T. Jing, Z. L. Wang, *Adv. Mater.* **2014**, *26*, 7432.
[6] Y. Yu, H. Sun, H. Orbay, F. Chen, C. G. England, W. Cai, X. Wang, *Nano Energy* **2016**, *27*, 275.
[7] Z. L. Wang, *Mater. Today* **2017**, *20*, 74.
[8] A. Ben Amar, A. B. Kouki, H. Cao, *Sensors* **2015**, *15*, 28889.
[9] V. Bhatnagar, P. Owende, *Energy Sci. Eng.* **2015**, *3*, 153.
[10] X. Chen, X. Li, J. Shao, N. An, H. Tian, C. Wang, T. Han, L. Wang, B. Lu, *Small* **2017**, *13*, 1.
[11] Z. L. Wang, R. Yang, J. Zhou, Y. Qin, C. Xu, Y. Hu, S. Xu, *Mater. Sci. Eng., R* **2010**, *70*, 320.
[12] Y. Zhang, Y. Liu, Z. L. Wang, *Adv. Mater.* **2011**, *23*, 3004.
[13] R. Yang, Y. Qin, L. Dai, Z. L. Wang, *Nat. Nanotechnol.* **2009**, *4*, 34.
[14] Z. L. Wang, J. Chen, L. Lin, *Energy Environ. Sci.* **2015**, *8*, 2250.
[15] S. Wang, L. Lin, Z. L. Wang, *Nano Lett.* **2012**, *12*, 6339.
[16] L. Lin, S. Wang, Y. Xie, Q. Jing, S. Niu, Y. Hu, Z. L. Wang, *Nano Lett.* **2013**, *13*, 2916.
[17] P. Bai, G. Zhu, Y. Liu, J. Chen, Q. Jing, W. Yang, J. Ma, G. Zhang, Z. L. Wang, *ACS Nano* **2013**, *7*, 6361.
[18] S. Niu, Y. Liu, S. Wang, L. Lin, Y. S. Zhou, Y. Hu, Z. L. Wang, *Adv. Funct. Mater.* **2014**, *24*, 3332.
[19] Y. Yang, H. Zhang, J. Chen, Q. Jing, Y. S. Zhou, X. Wen, Z. L. Wang, *ACS Nano* **2013**, *7*, 7342.
[20] S. Niu, S. Wang, Y. Liu, Y. S. Zhou, L. Lin, Y. Hu, K. C. Pradel, Z. L. Wang, *Energy Environ. Sci.* **2014**, *7*, 2339.
[21] S. Wang, S. Niu, J. Yang, L. Lin, Z. L. Wang, *ACS Nano* **2014**, *8*, 12004.
[22] S.-H. Shin, Y. H. Kwon, M. H. Lee, J.-Y. Jung, J. H. Seol, J. Nah, *Nanoscale* **2016**, *8*, 1314.
[23] G. Zhu, R. Yang, S. Wang, Z. L. Wang, *Nano Lett.* **2010**, *10*, 3151.
[24] S. Xu, Y. Qin, C. Xu, Y. Wei, R. Yang, Z. L. Wang, *Nat. Nanotechnol.* **2010**, *5*, 366.
[25] Y. Hu, Y. Zhang, C. Xu, G. Zhu, Z. L. Wang, *Nano Lett.* **2010**, *10*, 5025.
[26] S. Paria, S. K. Karan, R. Bera, A. K. Das, A. Maitra, B. B. Khatua, *Ind. Eng. Chem. Res.* **2016**, *55*, 10671.
[27] K. ParkII, M. Lee, Y. Liu, S. Moon, G. T. Hwang, G. Zhu, J. E. Kim, S. O. Kim, D. K. Kim, Z. L. Wang, K. J. Lee, *Adv. Mater.* **2012**, *24*, 2999.
[28] C. K. Jeong, K. ParkII, J. Ryu, G. T. Hwang, K. J. Lee, *Adv. Funct. Mater.* **2014**, *24*, 2620.
[29] J. Kwon, W. Seung, B. K. Sharma, S.-W. Kim, J.-H. Ahn, *Energy Environ. Sci.* **2012**, *5*, 8970.
[30] A. Wang, Z. Liu, M. Hu, C. Wang, X. Zhang, B. Shi, Y. Fan, Y. Cui, Z. Li, K. Ren, *Nano Energy* **2018**, *43*, 63.
[31] Z. Pi, J. Zhang, C. Wen, Z. bin Zhang, D. Wu, *Nano Energy* **2014**, *7*, 33.
[32] C. K. Jeong, K.-I. Park, J. H. Son, G.-T. Hwang, S. H. Lee, D. Y. Park, H. E. Lee, H. K. Lee, M. Byun, K. J. Lee, *Energy Environ. Sci.* **2014**, *7*, 4035.
[33] C. K. Jeong, J. H. Han, H. Palneedi, H. Park, G. T. Hwang, B. Joung, S. G. Kim, H. J. Shin, I. S. Kang, J. Ryu, K. J. Lee, *APL Mater.* **2017**, *5*, 074102, https://doi.org/10.1063/1.4976803.
[34] C. Zhang, W. Tang, C. Han, F. Fan, Z. L. Wang, *Adv. Mater.* **2014**, *26*, 3580.
[35] Q. Zheng, Y. Jin, Z. Liu, H. Ouyang, H. Li, B. Shi, W. Jiang, H. Zhang, Z. Li, Z. L. Wang, *ACS Appl. Mater. Interfaces* **2016**, *8*, 26697.
[36] N. Zhang, C. Tao, X. Fan, J. Chen, *J. Mater. Res.* **2017**, *32*, 1628.
[37] W. Xu, L. B. Huang, M. C. Wong, L. Chen, G. Bai, J. Hao, *Adv. Energy Mater.* **2017**, *7*, 1.
[38] M. Ma, Z. Zhang, Q. Liao, G. Zhang, F. Gao, X. Zhao, Q. Zhang, X. Xun, Z. Zhang, Y. Zhang, *Nano Energy* **2017**, *39*, 524.
[39] Q. Liang, Q. Zhang, X. Yan, X. Liao, L. Han, F. Yi, M. Ma, Y. Zhang, *Adv. Mater.* **2017**, *29*, 1604961, https://doi.org/10.1002/adma.201604961.
[40] G. D. Nelson, *Texas Heart Inst. J.* **1993**, *20*, 12.
[41] V. S. Mallela, V. Ilankumaran, S. N. Rao, *Indian Pacing Electrophysiol. J.* **2004**, *4*, 201.
[42] Z. Li, G. Zhu, R. Yang, A. C. Wang, Z. L. Wang, *Adv. Mater.* **2010**, *22*, 2534.
[43] G. T. Hwang, H. Park, J. H. Lee, S. Oh, K. ParkII, M. Byun, H. Park, G. Ahn, C. K. Jeong, K. No, H. Kwon, S. G. Lee, B. Joung, K. J. Lee, *Adv. Mater.* **2014**, *26*, 4880.
[44] M. Southcott, K. MacVittie, J. Halámek, L. Halámková, W. D. Jemison, R. Lobel, E. Katz, *Phys. Chem. Chem. Phys.* **2013**, *15*, 6278.
[45] C. Dagdeviren, B. D. Yang, Y. Su, P. L. Tran, P. Joe, E. Anderson, J. Xia, V. Doraiswamy, B. Dehdashti, X. Feng, B. Lu, R. Poston, Z. Khalpey, R. Ghaffari, Y. Huang, M. J. Slepian, J. A. Rogers, *Proc. Natl. Acad. Sci. USA* **2014**, *111*, 1927.
[46] Q. Zheng, B. Shi, F. Fan, X. Wang, L. Yan, W. Yuan, S. Wang, H. Liu, Z. Li, Z. L. Wang, *Adv. Mater.* **2014**, *26*, 5851.
[47] A. D. Krahn, R. A. Pickett, S. Sakaguchi, N. Shaik, J. Cao, H. S. Norman, P. Guerrero, *Pacing Clin. Electrophysiol.* **2014**, *37*, 505.
[48] Y. Ma, Q. Zheng, Y. Liu, B. Shi, X. Xue, W. Ji, Z. Liu, Y. Jin, Y. Zou, Z. An, W. Zhang, X. Wang, W. Jiang, Z. Xu, Z. L. Wang, Z. Li, H. Zhang, *Nano Lett.* **2016**, *16*, 6042.
[49] Q. Zheng, H. Zhang, B. Shi, X. Xue, Z. Liu, Y. Jin, Y. Ma, Y. Zou, X. Wang, Z. An, W. Tang, W. Zhang, F. Yang, Y. Liu, X. Lang, Z. Xu, Z. Li, Z. L. Wang, *ACS Nano* **2016**, *10*, 6510.
[50] D. H. Kim, H. J. Shin, H. Lee, C. K. Jeong, H. Park, G. T. Hwang, H. Y. Lee, D. J. Joe, J. H. Han, S. H. Lee, J. Kim, B. Joung, K. J. Lee, *Adv. Funct. Mater.* **2017**, *27*, 1700341.
[51] L. Y. Chen, B. C.-K. Tee, A. L. Chortos, G. Schwartz, V. Tse, D. J. Lipomi, H.-S. P. Wong, M. V. McConnell, Z. Bao, *Nat. Commun.* **2014**, *5*, 5028.
[52] P. A. Heidenreich, J. G. Trogdon, O. A. Khavjou, J. Butler, K. Dracup, M. D. Ezekowitz, E. A. Finkelstein, Y. Hong, S. C. Johnston, A. Khera, D. M. Lloyd-Jones, S. A. Nelson, G. Nichol, D. Orenstein, P. W. F. Wilson, Y. J. Woo, *Circulation* **2011**, *123*, 933.
[53] T. Sharma, S. S. Je, B. Gill, J. X. J. Zhang, *Sens. Actuators, A* **2012**, *177*, 87.
[54] O. H. Murphy, M. R. Bahmanyar, A. Borghi, C. N. McLeod, M. Navaratnarajah, M. H. Yacoub, C. Toumazou, *Biomed. Microdevices* **2013**, *15*, 737.
[55] C. Dagdeviren, Y. Shi, P. Joe, R. Ghaffari, G. Balooch, K. Usgaonkar, O. Gur, P. L. Tran, J. R. Crosby, M. Meyer, Y. Su, R. Chad Webb, A. S. Tedesco, M. J. Slepian, Y. Huang, J. A. Rogers, *Nat. Mater.* **2015**, *14*, 728.
[56] H. Zhang, X. Zhang, X. Cheng, Y. Liu, *Nano Energy* **2015**, *12*, 296.
[57] X. Cheng, X. Xue, Y. Ma, M. Han, W. Zhang, Z. Xu, H. Zhang, H. Zhang, *Nano Energy* **2016**, *22*, 453.
[58] D. Y. Park, D. J. Joe, D. H. Kim, H. Park, J. H. Han, C. K. Jeong, H. Park, J. G. Park, B. Joung, K. J. Lee, *Adv. Mater.* **2017**, *1702308*, 1.
[59] S. Munir, B. Jiang, A. Guilcher, S. Brett, S. Redwood, M. Marber, P. Chowienczyk, *Am. J. Physiol. Heart Circ. Physiol.* **2008**, *294*, H1645.
[60] H. Ouyang, J. Tian, G. Sun, Y. Zou, Z. Liu, H. Li, L. Zhao, B. Shi, Y. Fan, Y. Fan, Z. L. Wang, Z. Li, *Adv. Mater.* **2017**, *29*, 1703456.

[61] S. C. Millasseau, R. P. Kelly, J. M. Ritter, P. J. Chowienczyk, *Clin. Sci.* **2002**, *103*, 371.
[62] F. Pivatelli, M. dos Santos, G. Fernandes, M. Gatti, L. de Abreu, V. E. Valenti, L. C. M. Vanderlei, C. Ferreira, F. Adami, T. D. de Carvalho, C. B. de M. Monteiro, M. F. de Godoy, *Int. Arch. Med.* **2012**, *5*, 31.
[63] H. S. Mayberg, A. M. Lozano, V. Voon, H. E. McNeely, D. Seminowicz, C. Hamani, J. M. Schwalb, S. H. Kennedy, *Neuron* **2005**, *45*, 651.
[64] G. Deuschl, *N. Engl. J. Med.* **2006**, *355*, 896.
[65] G. Hwang, Y. Kim, J. Lee, S. Oh, C. K. Jeong, D. Y. Park, J. Ryu, H. Kwon, S.-G. Lee, B. Joung, D. Kim, K. J. Lee, *Energy Environ. Sci.* **2015**, *8*, 2677.
[66] K. T. Ragnarsson, *Spinal Cord* **2008**, *46*, 255.
[67] S. Lee, H. Wang, Q. Shi, L. Dhakar, J. Wang, N. V. Thakor, S. C. Yen, C. Lee, *Nano Energy* **2017**, *33*, 1.
[68] E. J. Bradbury, S. B. McMahon, *Nat. Rev. Neurosci.* **2006**, *7*, 644.
[69] X. Gu, F. Ding, D. F. Williams, *Biomaterials* **2014**, *35*, 6143.
[70] S. Wislet-Gendebien, G. Hans, P. Leprince, J.-M. Rigo, G. Moonen, B. Rogister, *Stem Cells* **2005**, *23*, 392.
[71] J. Ladewig, P. Koch, O. Brüstle, *Nat. Rev. Mol. Cell Biol.* **2013**, *14*, 225.
[72] W. Guo, X. Zhang, X. Yu, S. Wang, J. Qiu, W. Tang, L. Li, H. Liu, Z. L. Wang, *ACS Nano* **2016**, *10*, 5086.
[73] Y. Jin, J. Seo, J. S. Lee, S. Shin, H. J. Park, S. Min, E. Cheong, T. Lee, S. W. Cho, *Adv. Mater.* **2016**, *28*, 7365.
[74] M. B. Victor, M. Richner, T. O. Hermanstyne, J. L. Ransdell, C. Sobieski, P. Y. Deng, V. A. Klyachko, J. M. Nerbonne, A. S. Yoo, *Neuron* **2014**, *84*, 311.
[75] A. Gao, R. Hang, X. Huang, L. Zhao, X. Zhang, L. Wang, B. Tang, S. Ma, P. K. Chu, *Biomaterials* **2014**, *35*, 4223.
[76] H. Pretel, R. F. Z. Lizarelli, L. T. O. Ramalho, *Lasers Surg. Med.* **2007**, *39*, 788.
[77] W. Tang, J. Tian, Q. Zheng, L. Yan, J. Wang, Z. Li, Z. L. Wang, *ACS Nano* **2015**, *9*, 7867.
[78] M. Santosham, A. Chandran, S. Fitzwater, C. Fischer-Walker, A. H. Baqui, R. Black, *Lancet* **2010**, *376*, 63.
[79] R. Dastjerdi, M. Montazer, *Colloids Surf., B* **2010**, *79*, 5.
[80] C. D. Harvell, K. Kim, J. M. Burkholder, R. R. Colwell, P. R. Epstein, D. J. Grimes, E. E. Hofmann, E. K. Lipp, A. D. Osterhaus, R. M. Overstreet, J. W. Porter, G. W. Smith, G. R. Vasta, *Science* **1999**, *285*, 1505.
[81] C. Liu, X. Xie, W. Zhao, J. Yao, D. Kong, A. B. Boehm, Y. Cui, *Nano Lett.* **2014**, *14*, 5603.
[82] Q. Jiang, Y. Jie, Y. Han, C. Gao, H. Zhu, M. Willander, X. Zhang, X. Cao, *Nano Energy* **2015**, *18*, 81.
[83] J. Tian, H. Feng, L. Yan, M. Yu, H. Ouyang, H. Li, W. Jiang, Y. Jin, G. Zhu, Z. Li, Z. L. Wang, *Nano Energy* **2017**, *36*, 241.
[84] X. J. Zhao, J. J. Tian, S. Y. Kuang, H. Ouyang, L. Yan, Z. L. Wang, Z. Li, G. Zhu, *Adv. Mater. Interfaces* **2016**, *3*, 1600187.
[85] S. Xu, B. J. Hansen, Z. L. Wang, *Nat. Commun.* **2010**, *1*, 93.
[86] M. Irimia-Vladu, *Chem. Soc. Rev.* **2014**, *43*, 588.
[87] D.-H. Kim, J. Viventi, J. J. Amsden, J. Xiao, L. Vigeland, Y.-S. Kim, J. A. Blanco, B. Panilaitis, E. S. Frechette, D. Contreras, D. L. Kaplan, F. G. Omenetto, Y. Huang, K.-C. Hwang, M. R. Zakin, B. Litt, J. A. Rogers, *Nat. Mater.* **2010**, *9*, 511.
[88] Q. Zheng, Y. Zou, Y. Zhang, Z. Liu, B. Shi, X. Wang, Y. Jin, H. Ouyang, Z. Li, Z. L. Wang, *Sci. Adv.* **2016**, *2*, 1.
[89] C. Dagdeviren, Z. Li, Z. L. Wang, *Annu. Rev. Biomed. Eng.* **2017**, *19*, 85.
[90] P. Song, S. Kuang, N. Panwar, G. Yang, D. J. H. Tng, S. C. Tjin, W. J. Ng, M. B. A. Majid, G. Zhu, K. T. Yong, Z. L. Wang, *Adv. Mater.* **2017**, *29*, 1.
[91] J. Yang, J. Chen, Y. Su, Q. Jing, Z. Li, F. Yi, X. Wen, Z. Wang, Z. L. Wang, *Adv. Mater.* **2015**, *27*, 1316.
[92] D.-I. Kim, T. Quang Trung, B.-U. Hwang, J.-S. Kim, S. Jeon, J. Bae, J.-J. Park, N.-E. Lee, *Sci. Rep.* **2015**, *5*, 12705.

